RSC Advances

ROYAL SOCIETY OF CHEMISTRY

www.rsc.org/advances

Self-sacrifice Te Template Synthesis of New Phase $Pb_mSb_{2n}Te_{m+3n}$ Nanorods via Pb^{2+}/Sb^{3+} Synergistic Effect

Ziming Su[1,2], Qun Wang[1,2]*, Jianhuan Li[2], Guangjun Zhang[1]*

[1]State Key Laboratory of Advanced Welding and Joining, and [2]Department of Chemistry, Harbin Institute of Technology, 92 West Dazhi Street, Harbin, 150001, China.
E-mail:wangqun5992@hit.edu.cn;

Abstract: Nanocrystals have been attracted extra attention due to their unique characteristic different from their bulk counterparts. Herein, we first synthesized the new stable phase of ternary $Pb_mSb_{2n}Te_{m+3n}$ one-dimensional (1D) nanorods with rough surface, using Te as sacrificial template. X-ray diffraction technique (XRD), field emission scanning electron microscope (FE-SEM) and energy-dispersive spectroscopy (EDS), X-ray photoelectron spectroscopy (XPS) analysis have been used to characterize and determine the structure and composition of the product. By carefully adjusting the experimental conditions, it was found that reaction factors including distinct solvent, the amount of alkali, reaction temperature, the ratio of reactants and growth time, play critical roles in the crystallization process of $Pb_mSb_{2n}Te_{m+3n}$ nanorods. Thorough morphological characterizations revealed that significant variation of the morphology of products originated from varying the amount of Pb/Sb precursors injection. Reaction with excess Pb produces $Pb_mSb_{2n}Te_{m+3n}$ nanocubes having sizes variations, whereas the initial morphology of Te nanorod template with rough surface was preserved in the present of Sb. The Pb^{2+}/Sb^{3+} synergistic effect was attributed to the difference of their reaction reactivity. A mechanistic model is proposed to account for these experimental findings. Furthermore, the optical band gaps (*Eg*) of $Pb_mSb_{2n}Te_{m+3n}$ were investigated as well.

Key words: $Pb_mSb_{2n}Te_{m+3n}$; sacrificial template; Pb^{2+}/Sb^{3+}; synergistic effect.

1. Introduction

Tellurium, a narrow band semiconductor with a band gap of 0.3eV, has trigonal phase. In its crystal structure, Te atoms are believed to be bound together through Van der Waals interactions in a hexagonal lattice which leads to a very strong tendency towards anisotropic growth along the directions of [001], such as one-dimensional (1D) rods,[1] wires,[2] tubes[3] etc. Recently, these 1D Te nanostructures have further been utilized as a template for synthesizing different binary 1D metal telluride nanostructures. For instance, Jeong and his co-workers reported Te was transformed into Ag_2Te by topotactic transformation and further changed to diverse ultrathin chalcogenide nanowires M_xTe_y (M = Cd, Zn, Pb, and Pt) using a well-designed ion-exchange reaction,[4] in which CdTe can be also fabricated directly from Te as template.[5] Wu's research group have synthesized PbTe nanowires and Bi_2Te_3 nanowires and ultrathin metal telluride nanowires including Ag_2Te, $Cu_{1.75}Te$ and PbTe using safer reducing agent.[6,7] Meanwhile, Bi_2Te_3 nanowires can be obtained with cathodic stripping Te electrode by Yuan *et al*..[8] Besides the homogenous structure could be transformed from Te template, plenty of heterostructures have been reported by some research groups, such as PbTe-Bi_2Te_3,[9] Ag_2Te-Bi_2Te_3,[10] Te-Bi_2Te_3 nanostrings,[11] barbells,[12] core/shell nanotube[13]. That Te-Ag_2Te_3 had two kinds of structures was mostly due to two mechanism through the reactions that well-known Kirkendall effect or topotactic transformation.[14] Furthermore, Anirban Som *et al*. have prepared Ag_2Te nanowires or Ag-Te heterostructure controlled by the difference in reactivity of silver cluster in contrast to its ions and nanoparticles.[15] However, except for TeCuPt and PtPdTe nanowires,[16] efforts toward the facile synthesis and investigation of the ternary solid solution nanorods by Te templates had been rare.

Bulk lead telluride (PbTe), due to its narrow band gaps (0.32eV) and face-centered cubic structure, has been being applied widely in numbers of filed such as photovoltaic, IR photoelectric, thermoelectics.[17,18] In recent years, various morphology PbTe including quantum dots,[19] nanofilms,[18] nanosheets by self-assembling from nanoparticles,[20] porous microstructures,[21] nanocubes[17,22] hierachial nanostructures[23-25] and nanowires/nanorods[26] can be fabricated via varying multiple methods. On the other hand, alloying lead chalcogenides with a small amount of other semiconductor compounds for ternary or multinary compounds can increase the figure of merit through tuning the electrical transportant properties and the lattice thermal conductivity.[27-30] However, different from alloying bulk materials through high temperature solid state reaction, there have not been many

successes in the multinary PbTe-based semiconductor nanocrystals due to the "self-purification" of impurity,[31] especially those with small size. In the "self-purification" mechanism, the impurity formation energy in nanocrystals is much higher than that in bulk materials. Furthermore, from the kinetics perspective, the distance impurities need to travel to reach the surface of the nanocrystals is very small. Both of these facts cause a decrease of solubility of dopant impurities in nanocrystals.[31,32] Recently, there are increasing numbers of ternary or multinary compounds examples in multicomponent chalcogenide systems. For example, Mn-doped PbSe self-assembled by corresponding particles.[33] That Ag_2S acted as transposition state and obtained from Ag nanowires finally transformed to $AgFeS_2$ nanowires had researched by Yalcin *et al.*.[34] Ajay singh *et al.* doped Ga, Sb into CuInS with shape controlling via tuning dosage of Ga, catalyzed by antimony,[35] which was similar to PbSe-Bi nanorods assembled from PbSe particles using Bi as catalyst.[36] Kade *et al.* had synthesized PbTe with In doping to formulate In atoms are more likely to place lead (Pb) rather than to take the interstitial sites.[17]

In addition, interestingly, Hao *et al.*[37] had discovered the existence of stable ternary rocksalt-based compounds: $SrPb_3S_4$, $SrPbS_2$, and Sr_3PbS_4, in the PbS–SrS system, which were similar to $Pb_{2-x}Sn_xS_2$ nanocrystals proved to be phase separation in bulk phase.[38] Kanatzidis' group had synthesized nanoscale stabilization of new phases of $Pb_mSb_{2n}Te_{m+3n}$ nanoparticles[39] and $Pb_mSb_{2n}Se_{m+3n}$ flower-like nanocrystal.[40] New phase of homologous $Pb_mBi_{2n}Te_{3n+m}$ nanosheets were fabricated by Arindom Chatterjee *et al.*.[41] However, despite decades of investigations in understanding the growth mechanism of semiconductor nanostructures, the formation protocols of these multinary systems were not well known. The well-studied classical mechanism of nucleation followed by growth is mostly restricted to binary semiconductors but not appropriate to multinary structures.[42,43] To our best knowledge, there were still few literature studying stable new phases of $Pb_mSb_{2n}Te_{m+3n}$ exhibiting nanorod morphology to date except several phase shown in phase digram[39] (Fig. 1). $Pb_mSb_{2n}Te_{m+3n}$ nanorods can only exist in nanoscale, which have been proved to be PbTe-Sb_2Te_3 mixture in bulk except $PbSb_4Te_4$ and $PbSb_2Te_4$.

Herein, we had prepared stable 1D $Pb_mSb_{2n}Te_{m+3n}$ bamboo-like nanorods by solvothermal method via Te as sacrificial template. To the best of our knowledge, this was first time report of rod-shaped secondary structures. Two-step method that introduced Pb source and Sb source simultaneously after Te nanorod template had been generated completely was employed. The

shape-depending on dosages of Pb/Sb source had been discussed, which involved synergistic interaction between Pb^{2+} and Sb^{3+}. Moreover, the formation mechanism had also studied compared to one-step method during the chemical transformation.

2. Experimental Part

2.1 Synthesis

In a typical synthesis of $Pb_mSb_{2n}Te_{m+3n}$ nanorods with solvothermal procedure, 0.320g sodium selenite (Na_2TeO_3) and 0.250g ethylenediaminetetraacetic acid disodium salt (EDTA) was added into a beaker in which 10ml ethylene glycol had been. After constantly electromagnetic stirring for 10min with injection of 4mL hydrazine hydrate 80% ($N_2H_4 \cdot H_2O$), the mixture was transferred into a 20 mL stainless teflon-lined autoclave, sealed and maintained in an oven with the planned temperature of 180□ for 0.5h. The autoclave was cooled down to room temperature naturally after reaction and then 0.5g lead acetate ($Pb(CH_3COO)_2 \cdot 3H_2O$), a series of dosage of antimony potassium tartrate ($K(SbO)C_4H_4O_6 \cdot 0.5H_2O$, 0.3g for Sample 1; 1.0g for Sample 2; 1.5g for Sample 3), 0.3g potassium hydroxide (KOH) were added into a dry beaker, into which the products obtained above was transferred. After being stirred for 15 min until all of the chemicals were dispersed thoroughly, transferred them into a 20 mL stainless teflon-lined, kept heating under 180 for 5.5h and cooled to room temperature. After that, washed the sample prepared using pure water and ethanol for three times respectively, dried in a vacuum oven at 80 □ for 4 h finally. All of synthesis procedures and a part of photographs were shown in Fig. 2 and element composition measured by ICP-AES, lattice parameter, and mole Sb/ total mole (Sb+Pb) were shown in Table. 1.

2.2. Characterization.

The X-ray diffraction (XRD) patterns of the products collected at room temperature were performed on a Rigaku D/max-2000 diffractometer equipped with Cu Kα radiation from 20° to 80° with the step of 0.02° and scanning rate of 5°/min; a field emission scanning electron microscope (FESEM), energy-dispersive X-ray spectroscopy (EDS; Quanta 200F) and transmission electron microscopy, and high-resolution transmission electron microscopy (HRTEM, FEI, Tecnai G2 F30). Inductively coupled plasma-atomic emission spectroscopy (ICP-AES) was used to determine the elemental composition of the prepared series of $Pb_mSb_{2n}Te_{m+3n}$ nanocrystals. Only Pb^{2+} and Sb^{3+} were analyzed as Te is liberated as H_2Te gas during the dissolution process in *aqua regia*. The reported amounts of Te are only estimated, assuming charge-balanced compositions. The binding

energy and surface oxidation of the prepared products were explored on the X-ray photoelectron spectrometer (XPS) (PHI 5700 ESCA40), using Al K_α radiation as the exciting source. The optical property of the products was performed with a Fourier transform infrared spectrometer (FTIR, Nicolet 5700).

3.Results and Discussion

3.1 Structure and Morphology Characterization

The composition and phase of the as-prepared samples can be determined by the powder X-ray diffraction pattern (XRD), which was used to examine the crystal structure and the phase purity of materials whose XRD pattern is unique and definitely different from any others. As indicated in Fig. 3a, the $Pb_mSb_{2n}Te_{m+3n}$ samples synthesized by two-step method displayed pure phase and all the diffraction peaks can be indexed to PbTe with face-centered-cubic (*fcc)* structure with space group Fm-3m (225) (JCPDS#38-1435), in which presented some diffraction peaks that were (111), (200), (220), (311), (222), (400), (420), (422) and (511) planes corresponded to the 2θ of 23.8°, 27.7°, 39.4°, 46.6°,48.8°, 57°, 64.4°, 71.5°, 76.5°. The narrow and sharp peaks show its high crystallinity and no characteristic peaks peculiar to the source materials or other impurities were observed. As expected for the smaller ionic radius of Sb, (radius of Sb and Pb are ~1.45 Å and ~1.80 Å, respectively), a gradual shift to higher 2θ was observed (Fig. 3a) as the Sb content in the $Pb_mSb_{2n}Te_{m+3n}$ alloys increased.[44] The measured fined lattice parameters demonstrated a linear dependence as it decreased monotonically with increasing Sb content. This linear dependence was consistent with Vegard's law and demonstrated the compositional homogeneity of these $Pb_mSb_{2n}Se_{m+3n}$ alloys (shown in Fig. 3b). The Energy Dispersive Spectrometer (EDS) showed that the existence of the Sb atoms in PbTe matrix, which was consistent with XRD pattern(shown in Fig. 3c). Moreover, it determined the elemental composition of the prepared series of $Pb_mSb_{2n}Se_{m+3n}$ nanorods, whose data were similar to those measured by ICP-AES.

The morphology of the Sample 1 was studied by FESEM were shown in Fig. 4, in which the low-magnification SEM images presented overall morphology of the products with homogeneous dispersing, uniform size and high yield (Fig. 4a-b). As in the high-magnification images (Fig. 4c), a numbers of bamboo-like nanorods appeared, which were likely to be assembled by four or five small cubes with lengths of 200m-250nm and thickness of 40-50nm. 3D schematic diagram of such

bamboo-like nanorods was drawn in Fig. 4d. Moreover, the typical front-view line-scan EDS profile of a single nanorod, characterized by TEM (Fig. 4e), clearly displays that the presence of all expected Pb, Te and Sb elements in nanorod samples. The single phase homogeneity of the nanocrystals was further confirmed by the consistent rise and fall of Pb, Te, and Sb signals moving through the nanorods shown in the EDS line scan (inset in Fig. 4e). A HRTEM image taken from an the $Pb_mSb_{2n}Te_{m+3n}$ nanorod edge was displayed in Fig. 4f and it can be seen that the interfringe distance in the single crystalline region is 0.32 nm, corresponding to the lattice spacing of the (100) planes in the cubic structure, showing the nanorod axis is aligned with the [100] crystal direction. This is similar to the [200] axial direction observed in PbTe nanowires grown using two-step hydrothermal methods.[45,46]

To date, metal tellurides one dimensional nanostructures usually exhibited smooth or rough surface which was attributed to different chemical conversion mechanism under special synthetic conditions. Firstly, Fang *et al*. demonstrated that one dimensional (1D) corrugated nanoarrays of $Pb_{(1-x)}Mn_xSe$ nanocrystals through an in-situ self-assembly processes based on the fundamental building blocks of octahedral nanocrystals.[33] Pearl-necklace-shaped PbTe nanowires can be formed from the oriented attachment growth of spherical cubic PbTe nanoparticles and partially accompanied by Ostwald ripening to form partially smooth surface nanowires.[47] Secondly, ultrathin (<15 nm) PbTe and Bi_2Te_3 nanowires in a low-cost solution-based process using Te nanowire templates would not have rough surface due to short diffusion pathway and the released strain.[6,7] Thirdly, rough PbTe polycrystalline thermoelectric nanorods were fabricated through chemical transformation of Te nanorods.[48] Therefore, there was a question come to be raised, what morphology of the samples really be? Were they bamboo-like nanorods with semi-cube-like coarse surface or nanorods consisted of some senior cubes units? In order to solve this problem, the growth mechanism of the nanorods was going to be discussed in following part.

The quality and composition of the as-prepared samples were further studied by X-ray photoelectron spectroscopy (XPS) analysis. Fig. 5a showed the XPS of the Sample 1 and Sample 3 with high resolution spectra of O 1s, Pb 4f, Te 3d and Sb 3d. The peaks at 142.28eV and 137.43eV in the high-resolution Pb 4f corresponding to Pb $4f_{2/5}$ and $4f_{7/2}$ with shoulder peaks on the high binding energy side (143.38eV and 138.68eV shown in Fig. 5b). Two components at 137.43eV and 138.68eV can be deconvoluted by reconvolution curve fitting (Fig. 5c-d), which corresponded to the expected

chemical shifts for PbTe and either $Pb(OH)_2$ or PbO.[49] In addition, two sets of peaks at 540.13eV, 530.88eV were assigned to Sb $3d_{3/2}$ and Sb $3d_{5/2}$ respectively.[50] From the Fig. 5e, the binding energy of Sb 3d of Sample 3 was stronger than those of Sample 1, which was attribute to the increasing dosage of Sb precursors. Te 3d region had two groups of peaks, which were observed at 585.03eV and 574.33eV, indicating the existence of Te^{2-} and either PbTe or Sb_2Te_3, and Te^{4+} (586.78eV and 576.33eV) due to a surface oxide layer.[51] Notably, the oxide peaks of Sample 1 were stronger than that of Sample 3 shown in Fig. 5, we estimated that Sample 1 with rougher surface (Fig. 4c) would have higher surface/volume ratio, which suggested that Sample 1 can be oxidized in air atmosphere more easily than Sample 3, thereby increasing the proportion of PbO and Te^{4+} in Sample 1. Oxidation of PbTe is a complex, multistage process which is believed to start with the formation of peroxide-like structures and terminate in the formation of $PbTeO_3$ on exposure to large O_2 concentrations.[52] For continuous surface oxide growth, oxygen atoms need to diffuse into the crystal and locally distort the perfect crystal structure, increasing disorder on the surface. A significant amount of oxygen is usually observed at the surface of PbTe NPs when exposed to air even during very short periods of time.[53,54] In our case, large surface-to-volume ratio of nanorods showed high reaction reactivity with O_2, because the more dangling bonds of bare and uncoordinated metal sites (Pb, Sb) may exist due to extrinsic doping. Therefore, the surface of product was covered by the amorphous thin oxide layer.

3.2 Investigation of Parameters Influencing the Formation of $Pb_mSb_{2n}Te_{m+3n}$ nanorods

The shapes and structures of metal telluride (M_xTe_y) nanocrystals can be influenced by a series of factors including the choice of solvent, reaction temperature, surfactant, reaction time, thermal regime, the molar ratio of the starting materials, reducing agents and so on. Therefore, we conducted experiments to examine the factors affecting the morphologies change of products on different reaction conditions.

3.2.1 The influence of solvent

Recently studies have shown that the reaction solvent is the one of keys to be able to predictably control the crystal and film growth by affecting the reaction process for changing viscosity, polarity, ion transfer rate and other characters[55,56]. Herein, in order to explain the importance of ethylene

glycol (EG) in generating nanorod-shape of Sample 1, a group of experiments were conducted by varying the mixture solvents (mixing other solvents with EG) at different ratios while keeping other conditions constant. The influence of the solvents on the morphology and structure of crystals were examined by SEM (Fig. S1). Only plenty of nanocubes in sizes of 50-80nm appeared when used mixture solvent of Di-n-propylamine/EG and ethanediamine (EA)/EG at the ratio of $V_{Di\text{-}n\text{-}propylamine}$: V_{EG} = 1:1 and V_{EA}:V_{EG} = 1:1 (Fig. S1 a,b). As a mixed solvent ratio of EG and H_2O was V_{H_2O}:V_{EG}=1:1 and even used pure water as solvent, a mass of nanorods with smoother surface compared to the Sample 1 were obtained (Fig. S1 c,d). The interaction between solvent and solute, solvent and solvent, are a very important chemical property that has a large impact on the chemical reactions taking place. It can induce some complex reactions among different solvents and different reactants, which finally leads to the existence of various structures and shapes. Non-aqueous solvent with higher viscosity allows the self-assemblies to occur at different rates, forming various morphologies in different solvents,[57,58] which affects the solubility, reactivity and diffusion behavior of the reagents and the intermediates.[59] Thus, given what we had discussed above, it was apparent that an optimal mixed solvent is indispensable to the formation of the $Pb_mSb_{2n}Te_{m+3n}$ and it was clearly seen that the bamboo-like rods could only be synthesized by using pure EG as solvent.

3.2.2 Effect of Temperature

The synthetic temperature, as one essential reaction parameter, can have an obvious influence on the shapes and structures of the final products. Some literatures had been reported that the morphologies and sizes of PbTe crystals are sensitive to the synthetic temperature. For example, Wang's research group had obtained different shapes of PbTe including tiny particles, nanocubes, nanocubes with spiral steps and dendrites with spirial step hollow cubic centers via ranging temperature from 100□ to 160□.[24] In our case, distinct morphologies can be fabricated at 120□, 140□ and 200□ respectively without changing any other experimental conditions (Fig. 6). When the reaction temperature was 120□, SEM images revealed that nanopores were obviously observed throughout the nanorods (Fig. 6a-b). Increasing temperature to 140□, the mixtures of nanorods and broken nanotubes acquired instead (Fig. 6c). Both nanorods and nanotubes had disappeared and some nanocubes with the sizes about 1μm could be observed when the temperature was up to 200℃ (Fig. 6d).

On the basis of the above experimental results, porous nanotubes were favorable to be obtained at lower temperature due to the nanoscale Kirkendall effect. The nanoscale Kirkendall Effect is a general phenomenon[60,61] and this research field had recently been reviewed by Wang *et al*..[62] As we known, the different diffusion rates of Te outward from internal of nanorods and Pb^{2+}/Sb^{3+} inward directly caused hollow structures. It is well known that EDTA or ethylenediaminetetraacetic acid is a novel molecule for complexing metal ions. The formation constant for Pb-EDTA complex is reported to be 10.[63] Pb^{2+}/Sb^{3+} could react with EDTA to form relative stable [Pb(EDTA)] and $[Sb(EDTA)^{+}]$ complex. It suggested that Pb^{2+}/Sb^{3+} diffusion rates inward would be slower than Te diffuse outward because of the generation of isolated high active Pb/Sb ions had been suppressed. Pb/Sb ions first selectively nucleated at the side surface of the Te nanowires, which subsequently caused the formation of a Pb/Sb−Te alloy layer on the surface on Te nanowires, non-equalizing diffusion between Pb/Sb and Te through the layer leaded to void formation between the Pb/Sb−Te alloy layer and the core Te nanowires. Next, the Te core nanowires disappear through continuous mass transport and highly crystalline nanotubes were finally obtained. Raising the temperature to 140□, [Pb(EDTA)] and $[Sb(EDTA)^{+}]$ complex can greatly accelerate the generation of Pb/Sb ions. According to the Fick Rules : $J= -D(dC/dx)$, J is diffusion flux, D is diffusion coefficient, (dC/dx) is refined as concentration gradient. In this case, J increased due to the improvement of concentration gradient caused by releasing mass of Pb/Sb ions from the coordination compound, thereby leading to the fast diffusion of Pb^{2+}/Sb^{3+} inward into the Te matrix. On the other hand, the rate of the ions diffusion was relatively fast with respect to that of crystal growth, upon the ion-exchange reaction, solid nanorods become nanoporous hollow rod-like products. At higher temperature of 200□, Te nanorods had a quick tendency to dissolve into Te^{2-} in based environment. Of course, another possibility should be considered is lower melting points of Te nanorods than those of Te bulk (421 °C). Then, Pb-Sb-Te cubes/particles can generate between Te^{2-} with Pb^{2+}/Sb^{3+} directly through homogeneous nucleation. In our present work, different shaped crystals may be related to the diffusion rate of the ions and the growth rate of the crystals based on the concentration gradient around the interface of Te nanorods. Thus, the optimal reaction was maintained at 180 °C for 5.5 h which can lead to the uniform and nearly bamboo-like pure $Pb_mSb_{2n}Te_{m+3n}$ nanorods.

3.2.3 Effect of the Amount of KOH

Besides the synthetic temperature discussed above, the amount of OH ions is another reaction factor which played significant roles in the fabrication of the $Pb_mSb_{2n}Te_{m+3n}$ crystals. Herein, a group of experiments were designed except for the variation of KOH concentrations. All the samples were prepared under the same reaction conditions as shown in the typical synthesis process. Without KOH, several smooth nanorods were observed shown in Fig. 7a-b. Whereas, the amount of KOH was 0.1g (1.79 mmol), the nanorods with small fractures appeared be coarse (Fig. 7c). Furthermore, increasing the amount of KOH to 1.5g (26.79 mmol) (Fig. 7d), a plenty of nanorods were obtained instead. It was reasonable to conclude that the amount of KOH played crucial role in reaction equilibrium existed in the following reaction process.

$$3TeO_3^{2-}+3N_2H_4 \rightarrow 3Te+3N_2+3H_2O+6OH^- \quad (1)$$

$$3Te+6OH^- \rightarrow 2Te^{2-}+TeO_3^{2-}+3H_2O \quad (2)$$

Firstly, TeO_3^{2-} had been reduced by $N_2H_4{\cdot}H_2O$ and sufficient Te atoms with high activity had been prepared according to Eq. 1 and the OH ions could transform Te into Te^{2-} and corrode the Te nanorods according to Eq. 2. When the reaction was carried out without OH ions, the chemical reaction route was mainly Eq1, and the samples could maintain the nanorod shape via heterogeneous nucleation. When a little KOH existed in the reaction system, Te atoms were partly converted into Te^{2-} and TeO_3^{2-} through Eq. 2, which caused some fractures generated on the surface. When excessive KOH were added, Te^{2-} and TeO_2^{3-} were continuously generated and subsequently nanocubes were obtained through homogeneous nucleation in which Te^{2-} reacted with Pb^{2+}/Sb^{3+}. Based on the above discussions, we can conclude that KOH used in the preparation would play vital roles in adjusting chemical reaction route and further influencing the nucleation and growth of $Pb_mSb_{2n}Te_{m+3n}$ nanostructures.

3.2.4 Effect of the Amount of Metal Precursors

The presence of Pb and Sb precursors, as reactant reacted with parent Te nanorods at first step, can finally generate the target products. Varying the amount of Sb precursors had been investigated and shown in Fig. 8. When Sb precursors were absent, Te nanorods only reacted with Pb and finally generated a number of nanocubes in sizes of 50~100nm (Fig. 8a). Unquestionably, PbTe nanocrystals, as we known, posses an average NaCl structure with a mix of eight {111} and six {100} faces to

minimize the total surface energy and its crystallite is determined by the ratio the growth rate of the [100] to that of [111]. As the result of the intrinsic surface energy of (111) face is higher than all of the {100} face, PbTe cubes are more likely to be obtained due to faster growth rate in the (111) face. If the amount of Sb precursors increased to 1.0g (Fig. 8b, Sample 2), the nanorods were smoother than the Sample 1. With further rising of the amount of Sb precursors to 1.5g (Fig. 8c, Sample 3), nanorods with smoother surface can be seen. However, in the presence of excess Sb precursors (2.0g) (Fig. 8d), it was clearly that the mixture of several hexagonal plates (marked by arrows) and a mass of nanocubes in sizes of 30~50nm appeared. Sb_2Te_3 prefer to present hexagonal plates due to their layer crystal structure in some previously literatures.[11,64] No matter how the amount of Sb precursors increasing (0.3g~1.5g), the samples were PbTe phase indicating Sb atoms were more likely to replace Pb and incorporated into PbTe matrix. Clearly, the introduction of Sb precursors would evoke the competition reaction between Pb^{2+} / Sb^{3+} and Te nanorods. Here, the existence of Sb resources could occupy a number of reaction sites on the Te nanorods and block the pathway of Pb ions from one position to another. Therefore, antimony could perform as a kind of "inactive ions" compared to Pb ions. Previous study by R. J. Behm et al's work had revealed Ag atom was reduced due to the effect of site blocking (surface diffusion barrier) by the Sb atoms.[65] This reduces the Ag diffusion constant linearly with the amount of Sb. Consequently, the main reaction (Eq. 3) then had been suppressed and further decreased the rate of heterogeneous nucleation, which restrained forming cubic crystal structures and kept the morphologies of nanorods unchanged. Furthermore, it seemed that there would be a threshold value of the amount of Sb precursors, which can evoke the Eq. 4 generating in quantity. Meanwhile, the nanocubes in sizes of 30nm~50nm (Fig. 9d insert) were smaller than the counterparts without Sb precursors adding (about 50nm shown in Fig. 9a), which was attributed to the consummation of Te via the Eq. 4. Above all, different amount Sb precursors can influence the reaction and finally determine the shapes and structures of the products.

$$3Te + 2Pb^{2+} + 6OH^- \rightarrow 2PbTe + TeO_3^{2-} + 3H_2O \quad (3)$$

$$6Te + 3N_2H_4 + 4Sb^{3+} + 12OH^- \rightarrow 2Sb_2Te_3 + 3N_2 + 12H_2O \quad (4)$$

In order to further investigate the role of metal precursors in forming bamboo-like nanorods, varying the amount of Pb precursors with a fixed concentration of Sb^{3+} were performed. As increasing the amount of Pb from 0g to 0.5g, the products shape evolved from hexagonal plates with a number of spherical particles to bamboo-like nanorods (Fig. 8e). Based on XRD result (Fig. 8f), the

powders obtained in the absence of Pb precursors were corresponded to Sb_2Te_3 (PDF#72-1990) and excess Te (PDF#36-1452). As the Pb concentration was further increased from 1.0g to 1.5g (Fig. 8g-h), most of the nanocrystals were nanocubes in sizes of about 50nm. It was similar to the case of Sb absenting, in which excess Pb^{2+} would generate strong ion diffusion and show higher reaction activity toward Te nanorods, resulting in the nanocubes. Obviously, bamboo-like nanorods can't form in the presence of Pb^{2+} or Sb^{3+} alone. We cannot ignore anyone's role in tuning the nanocrystals morphology forming the bamboo-like nanorods due to synergistic interaction between Pb and Sb. Recent studies showed that the incorporation of dopants into the host lattices not only altered the composition of the nanocrystals but also modified nanocrystal nucleation and growth rates, ultimately impacting the final morphology of nanocrystal. Through adsorption onto the growth facets and tuning rate of the chemical reaction processes, dopants can catalyze or slow down or even stop the directional growth of the nanomaterials, and they can also change the phase as well as shape of some nanostructures. Recently, this impact of Sb on the reactivity of the gallium precursor may prove useful for synthesis of $CuIn_{1-x}Ga_xS_2$ (CIGS) nanocrystals.[35] By systematically tuning the amount of Sb^{3+} ion added, the influence of the dopant on shape is indirect; antimony catalyzes the incorporation of gallium. In our present work, the diffusivity and chemical reactivity of the Pb adatoms on the Te nanorod is reduced when the Sb atoms, even low amount of Sb precursor, act as repulsive impurities. Actually, based on the SEM images observed in Fig. 8a-d, the surface of the synthesized solid solution $Pb_mSb_{2n}Te_{m+3n}$ nanorod tends to be smoother with the increase the amount of Sb precursor. Of course, a minimum Sb ratio determining the switch of nanocube and nanorod need further investigate in the future. Consequently, generating the bamboo-like shapes need two essential factors. Firstly, Pb and Sb sources must co-exist to react with Te nanorods via cooperative effect. Secondly, it was necessary to keep the dosage of Pb and Sb sources being in a reasonable range, which was able to control the ion diffusion and reaction activity toward Te, leading to retain the shape of parent nanorod template.

4. Growth Mechanism.

It was quite obvious that the reaction during the second step had an important influence on the final structure. What happened after Pb/Sb precursors adding into the reaction system and which structure the products should be? Were they transformed from the Te nanorods or assembled by some

little nanocubes? Thus, two hypothesis about the mechanisms of $Pb_mSb_{2n}Te_{m+3n}$ crystal growth had been put forward (Fig. 9): (1) The alkali existed in the solution corrode the Te nanorods constantly until Te atoms were transformed into Te^{2-} that could react with Pb^{2+}/Sb^{3+} to generate $Pb_mSb_{2n}Te_{m+3n}$ nanocube through homogeneous nucleation. With the reaction going on, $Pb_mSb_{2n}Te_{m+3n}$ nanorods have been gotten involve the spontaneous arrangement and alignment of $Pb_mSb_{2n}Te_{m+3n}$ nanocubes via oriented attach process. (2) Pb / Sb ions diffused into the Te structure and reacted with Te to form PbTe phase in Te matrix via topotactic transformation.

To further understand what is the growth mechanism of such Sample 1 bamboo-like nanorods? A time-dependent experiment in the second step was carried out. Before the conversion, Te nanorods were produced and analyzed at the first step according to the Eq.1. From the SEM images, it can be seen that the Te products had 1D acicular nanorod with relatively smooth surface, which had a 500mm average length and 50nm average diameter (Fig. 10a). Trigonal tellurium (t-Te) tends to grow the one-dimensional structures with growing along the c-axis due to its highly anisotropic crystal structure consisting of helical chains of covalent boned atoms. The XRD pattern (Fig. 10b) can be indexed to be Te without any other impurity. At the initial stage (2h) (Fig. 10c), the products composed of small regular smooth rods. With the increase of growth period to 4h (Fig. 10d), it was beginning to appear bamboo-like nanorods with pits due to some topotactic transformation had taken place and make surface cracking. When Pb ions were incorporated into the Te nanorods from the outside to inside to form PbTe phase, the [001]-directed hexagonal Te was transformed into [111]-directed *fcc*. It made the angle between Te and Te atoms changed from 120° to 90° at <110> plane, perpendicular to c-axis, thereby leading to a large lattice strain. The accumulated stress was released by cracking the surface and even breaking the nanorods during the transformation and generating shorter nanorods, which can be proved by the SEM images that the as-prepared products with the average length of 250nm were shorter than Te nanorods with the average length of 500nm (Fig. 10e-f). Subsequently, after 8h, there were two structures co-existed: nanorods and nanocubes that the cracked surface further broke into (Fig. 10g). Finally, when the reaction time was extended to 72h, the pits developed into larger and deeper holes and the nanorods broke into a mass of nanocubes completely via relieving the lattice strain accumulated during topotactic transformation (Fig. 10h).

For the hypothesis (1): The Te nanorods were deconstructed by KOH to generate Te^{2-} reacting with Pb^{2+}/Sb^{3+} undoubtedly denied the importance of the first step which generated Te nanorods and

which was separated from the second step. Based on the above results, hypothesis (1) had been excluded. In addition, to further invalidated this hypothesis, one-pot method was investigated and its SEM image show in Fig. S2. The existence of plentiful nanocubes rather than nanorods we designed to can also demonstrate that it was not suit for hypothesis 1 in this system. Therefore, the present chemical transformation was based on hypothesis 2 through topotactic transformation.

On the basis of experimental results, different crystals morphologies were shown in Fig. 11. It indicated $Pb_mSb_{2n}Te_{m+3n}$ structures with certain morphology had the same tendency, they performed as different morphologies from 1D nanorod / tube to 3D nanocubes, as increasing the amount of KOH, time and temperature respectively. Whereas, the more details about the reaction mechanism need further clarifications.

5. Optical properties

To further study the optical properties of the $Pb_mSb_{2n}Te_{m+3n}$ nanorods obtained in typical synthesis route, they were investigated with FI-IR spectrometer and exhibited well-defined band gap energies shown in Fig. 14. The electronic transition between valence band and conduction band for a direct band-gap material is given by $(\alpha h\upsilon)^2 \sim (h\upsilon - Eg)$, in which "α" is the optical absorption coefficient, "*h*" is the Planck's constant, "*υ*" is the frequency of the incident radiation, "*hυ*" is the incident photon energy and "*Eg*" is Energy gap. *Eg* can be estimated by extending the liner part of the curve to zero absorption (Fig. 12). The band gap value of the Sample 1, Sample 2 and Sample 3 can be calculated to be 0.316eV, 0.341eV, 0.375eV, respectively. These band gap values were all bigger than previously reported value for binary PbTe dendritic structures (0.272 eV) ,[66] hopper crystal (0.268 eV) and nanowires (0.308 eV) in our previous work.[25] On the other hand, the band-gap energies of the $Pb_mSb_{2n}Te_{m+3n}$ nanorods are significantly smaller than the literature value in the range of 0.41-0.45 eV for ternary $Pb_mSb_{2n}Te_{m+3n}$ nanocrystals with particle size of 10-12 nm and that of pure PbTe nanocrystals with the size of about 10 nm (~0.43 eV).[39] By comparison, these values are significantly different from the band gaps of the individual binary end members are 0.28 eV for PbTe and 0.11eV for Sb_2Te_3 and two distinct PbTe-based compounds $PbBi_2Te_4$ and $PbBi_6Te_{10}$ samples (0.7 and 0.25 eV), respectively. [41] Interestingly, the band gap value of Sample 1 is closed to the literature value (0.31 eV) for PbTe nanoparticles prepared by Zhu's research group and the latter are expected to be blue-shifted by quantum confinement relative to its bulk parent.[67] Meanwhile, it was clearly

observed that Sample 3 showed higher band gap value than those of Sample 1 and Sample 2, which has been widely accepted that the amount of dopant increase is accompanied by changes in the optical properties.[68] In fact, it is well known that PbTe has a largest Bohr radius compared to any crystalline semiconductor. Especially, the anisotropy in PbTe is quite pronounced and quantum confinement effects will be felt in PbTe NCs with longitudinal Bohr radius (152 nm). [69]

4. Conclusion

In summary, we first put forward a solvothermal method to synthesize the metastable nanoscale phase $Pb_mSb_{2n}Te_{m+3n}$ ($Pb_{12..44}SbTe_{13.94}$, $Pb_{5.84}SbTe_{7.34}$, $Pb_{2.91}SbTe_{4.41}$) nanorods. $Pb_{12..44}SbTe_{13.94}$ bamboo-like nanorods were formed through topological transformation instead of assembled by several individual nanocubes. The products can only been gained via two-step method rather than one-step method. Sb precursors can occupy the site that should have been occupied by Pb and block the Pb diffuse way, thereby leading to the nanorod shape. The interfacial interaction between Pb, Sb species and Te crystal surface can successfully change the growth nature of crystals due to Pb^{2+}/Sb^{3+} synergistic effect. Due to the strong quantum confinement effect, the band gap value of the Sample 1, Sample 2 and Sample 3 can calculated to be 0.316eV, 0.341eV, 0.375eV, respectively. The method may be extended to the control of crystallization and formation of other one-dimensional multicomponent PbTe-based alloy compounds.

Acknowledgements

This work was supported by the National Natural Science Foundation of China (Project No. 21101044), Independent Subject of State Key Laboratory of Advanced Welding and Joining and the Fundamental Research Funds for the Central Universities (Grant No. HIT. NSRIF. 2013076 and IBRSEM. 201330).

Reference

1. Z. Liu, Z. Hu, J. Liang, S. Li, Y. Yang, S. Peng and Y. Qian, *Langmuir*, 2004, **20**, 214.

2. Y. J. Zhu, W. W. Wang, R. J. Qi and X. L. Hu, *Angew. Chem. Int. Ed.*, 2004, **116**, 1434.

3. A. Qin, Y. Fang, P. Tao, J. Zhang and C. Su, *Inorg.Chem.*, 2007, **46**, 7403.

4. G. D. Moon, S. Ko, Y. Xia and U. Jeong, *ACS Nano*, 2010, **4**, 2307.

5. H. W. Liang, S. Liu, Q. S. Wu and S. H. Yu, *Inorg. Chem.*, 2009, **48**, 4927.

6. S. W. Finefrock, H. Fang, H. Yang, H. Darsono and Y. Wu, *Nanoscale*, 2014, **6**, 7872.

7. H. Yang, S. W. Finefrock, J. D. Albarracin Caballero and Y. Wu, *J. Am. Chem. Soc.*, 2014, **136**, 10242.

8. G. Yuan, Y. Li, N. Bao, J. Miao, C. Ge and Y. Wang, *Mater. Chem. Phys.*, 2014, **143**, 587.

9. H. Fang, T. Feng, H. Yang, X. Ruan and Y. Wu, *Nano Lett.*, 2013, **13**, 2058.

10. H. Fang, H. Yang and Y. Wu, *Chem. Mater.*, 2014, **26**, 3322.

11. Y. Zhang, H. Chen, Z. Li, T. Huang and S. Zheng, *J. Cryst. Growth*, 2015, **421**, 13.

12. W. Wang, J. Goebl, L. He, S. Aloni and Y. Hu, *J. Am. Chem. Soc.*, 2010, **132**, 17316.

13. Z. Li, S. Zheng, T. Huang, Y. Zhang, R. Teng and G. Lu, *J. Alloy Compd.*, 2014, **617**, 247.

14. K.-R. Park, S. Kim, N. V. Myung, S.-O. Kang and Y.-H. Choa, *RSC Adv.*, 2015, **5**, 29782.

15. A. Som, A. K. Samal, T. Udayabhaskararao, M. S. Bootharaju and T. Pradeep, *Chem. Mater.*, 2014, **26**, 3049.

16. H. Li, C. Ren, S. Xu, L. Wang, Q. Yue, R. Li, Y. Zhang, Q. Xue and J. Liu, *J. Mater. Chem. A*, 2015, **3**, 5850.

17. K. Kadel, L. Kumari, X. Wang, W. Li, J. Y. Huang and P. P. Provencio, *Nanoscale Res. Lett.*, 2014, **9**, 227.

18. J. Si, J. Zhao, G. Ding and H. Wu, *Appl. Surf. Sci.*, 2014, **321**, 233.

19. A. Khiar, M. Eibelhuber, V. Volobuev, M. Witzan, A. Hochreiner, H. Groiss and G. Springholz, *Opt. Lett.*, 2014, **39**, 6577.

20. T. J. Zhu, X. Chen, X. Y. Meng, X. B. Zhao and J. He, *Cryst. Growth Des.*, 2010, **10**, 3727.

21. P. K. Rawat and P. Banerji, *RSC Adv.*, 2014, **4**, 29818.

22. J. Zhou, Z. Chen and Z. Sun, *Mater. Res. Bull.*, 2015, **61**, 404.

23. Z. Quan, Z. Luo, Y. Wang, H. Xu, C. Wang, Z. Wang and J. Fang, *Nano Lett.*, 2013, **13**, 3729.

24. Q. Wang, G. Chen and H. Yin, *J. Mater. Chem. A*, 2013, **1**, 15355.

25. H. Yin, Q. Wang and G. Chen, *Chem. Eng. J.*, 2014, **236**, 131.

26. S. W. Finefrock, G. Zhang, J. H. Bahk, H. Fang, H. Yang, A. Shakouri and Y. Wu, *Nano Lett.*, 2014, **14**, 3466.

27. L. D. Zhao, S. H. Lo, J. He, H. Li, K. Biswas, J. Androulakis, C. I. Wu, T. P. Hogan, D. Y. Chung, V. P. Dravid and M. G. Kanatzidis, *J. Am. Chem. Soc.*, 2011, **133**, 20476.

28. L. D. Zhao, J. He, S. Hao, C. I. Wu, T. P. Hogan, C. Wolverton, V. P. Dravid and M. G. Kanatzidis, *J. Am. Chem. Soc.*, 2012, **134**, 16327.

29. K. Biswas, J. He, Q. Zhang, G. Wang, C. Uher, V. P. Dravid and M. G. Kanatzidis, *Nat. Chem.*, 2011, **3**, 160.

30. K. Biswas, J. He, I. D. Blum, C. I. Wu, T. P. Hogan, D. N. Seidman, V. P. Dravid and M. G. Kanatzidis, *Nature*, 2012, **489**, 414.

31. G. M. Dalpian and J. R. Chelikowsky, *Phys. Rev. Lett.*, 2006, **96**. 226802.

32. M. H. Du, S. C. Erwin, A. L. Efros and D. J. Norris, *Phys. Rev. Lett.*, 2008, **100**, 179702.

33. W. Lu, P. Gao, W. B. Jian, Z. L. Wang and J. Fang, *J. Am. Chem. Soc.*, 2004, **126**, 14816.

34. B. Sciacca, A. O. Yalcin and E. C. Garnett, *J. Am. Chem. Soc.*, 2015, **137**, 4340.

35. A. Singh, A. Singh, J. Ciston, K. Bustillo, D. Nordlund and D. J. Milliron, *J. Am. Chem. Soc.*, 2015, **137**, 6464.

36. M. S. Kim and Y. M. Sung, *CrystEngComm*, 2012, **14**, 1948.

37. S. Hao, L. D. Zhao, C. Q. Chen, V. P. Dravid, M. G. Kanatzidis and C. M. Wolverton, *J. Am. Chem. Soc.*, 2014, **136**, 1628.

38. R. B. Soriano, C. D. Malliakas, J. Wu and M. G. Kanatzidis, *J. Am. Chem. Soc.*, 2012, **134**, 3228.

39. R. B. Soriano, I. U. Arachchige, C. D. Malliakas, J. Wu and M. G. Kanatzidis, *J. Am. Chem. Soc.*, 2013, **135**, 768.

40. R. B. Soriano, J. Wu and M. G. Kanatzidis, *J. Am. Chem. Soc.*, 2015, **137**, 9937.

41. A. Chatterjee and K. Biswas, *Angew. Chem. Int. Ed.* , 2015, **54**, 5623.

42. F. Wang, V. N. Richards, S. P. Shields and W. E. Buhro, *Chem. Mater.*, 2014, **26**, 5.

43. G. Jia and U. Banin, *J. Am. Chem. Soc.*, 2014, **136**, 11121.

44. H. S. Dow, M. W. Oh, B. S. Kim, S. D. Park, B. K. Min, H. W. Lee and D. M. Wee, *J. Appl. Phys.*,

2010, **108**, 113709

45. G. a. Tai, B. Zhou and W. Guo, *J. Phys. Chem. C*, 2008, **112**, 11314.

46. G. Xi, C. Wang, X. Wang, Y. Qian and H. Xiao, *J. Phys. Chem. C*, 2008, **112**, 965.

47. G. Tai, W. Guo and Z. Zhang, *Cryst. Growth Des.*, 2008, **8**, 2906.

48. X. Chen, T. J. Zhu and X. B. Zhao, *J. Cryst. Growth*, 2009, **311**, 3179.

49. G. H. Dong and Y. J. Zhu, *Chem. Eng. J.*, 2012, **193**, 227.

50. M. Hu, Y. Jiang, W. Sun, H. Wang, C. Jin and M. Yan, *ACS Appl. Mater. Interfaces*, 2014,**6**,19449.

51. J. W. Liu, J. H. Zhu, C. L. Zhang, H. W. Liang and S.-H. Yu, *J. Am. Chem. Soc.*, 2010, **132**,8945.

52. L. V. Yashina, T. S. Zyubina, R. Puttner, A. S. Zyubin, V. I. Shtanov and E. V. Tikhonov, *J. Phys. Chem. C*, 2008, **112**, 19995.

53. M. Scheele, N. Oeschler, I. Veremchuk, S.-O. Peters, A. Littig, A. Kornowski, C. Klinke and H. Weller, *ACS Nano.*, 2011, **5**, 8541.

54. Y. Zhao and C. Burda, *ACS Appl. Mater. Interfaces*, 2009, **1**, 1259.

55. K. Ding, H. Lu, Y. Zhang, M. L. Snedaker, D. Liu, J. A. Macia-Agullo and G. D. Stucky, *J. Am. Chem. Soc.*, 2014, **136**, 15465.

56. S. Mourdikoudis and L. M. Liz-Marzán, *Chem. Mater.*, 2013, **25**, 1465.

57. J. F. Banfield, S. A. Welch, H. Zhang, T. T. Ebert and R. L. Penn, *Science*, 2000, **289**, 751.

58. C. Schliehe, B. H. Juarez, M. Pelletier, S. Jander, D. Greshnykh, M. Nagel, A. Meyer, S. Foerster, A. Kornowski, C. Klinke and H. Weller, *Science*, 2010, **329**, 550.

59. W. S. Sheldrick and M. Wachhold, *Angew. Chem. Int. Ed.*, 1997, **36**, 206.

60. A. Cabot, M. Iba˜ez, P. Guardia and A. P. Alivisatos, *J. Am. Chem. Soc.*, 2009, **131**, 11326.

61. K. Y. Niu, J. Park, H. Zheng and A. P. Alivisatos, *Nano Lett.*, 2013, **13**, 5715.

62. W. Wang, M. Dahl and Y. Yin, *Chem. Mater.*, 2013, **25**, 1179.

63. Y. Li and A. E. Martell, *Inorg. Chim. Acta.*, 1995, **159**, 231.

64. H. Q. Yang, L. Miao, C. Y. Liu, C. Li, S. Honda, Y. Iwamoto, R. Huang and S. Tanemura, *ACS Appl. Mater. Interfaces*, 2015, **7**, 14263.

65. V. d. V. HA, V. J and B. R. J, *Phys. Rev. B*, 1998, **57**, 4127.

66. G. R. Li, C. Z. Yao, X. H. Lu, F. L. Zheng, Z. P. Feng, X. L. Yu, C. Y. Su and Y. X. Tong, *Chem. Mater.*, 2008, **20**, 3306.

67. T. J. Zhu, X. Chen, Y. Q. Cao and X. B. Zhao, *J. Phys. Chem. C*, 2009, **113**, 8085.

68. Y. Liang, L. Zhai, X. Zhao and D. Xu, *J. Phys. Chem. B*, 2005, **109**, 7120.

69. J. E. Murphy, M. C. Beard, A. G. Norman, P. Ahrenkiel, J. C. Johnson, P. Yu, O. I. Mic, A. J. Nozik and R. J. Ellingson, *J. Am. Chem. Soc.*, 2008, **20**, 3306.

Figure captions

Fig. 1 Pseudobinary phase diagram of the PbTe-Sb_2Te_3 system.

Fig. 2 (a) Schematic diagram of reaction temperature vs. time during the synthesis of $Pb_mSb_{2n}Te_{m+3n}$ nanorods. (b) Digital photos before and after injecting $N_2H_4 \cdot H_2O$. The solution in the beaker turned into black, showing the reduction reaction occurred.

Table. 1 Element composition, lattice parameter, and mole Sb/ total mole (Sb+Pb).

Fig. 3 (a) Comparative XRD patterns of $Pb_mSb_{2n}Te_{m+3n}$ solid solution samples and a standard PbTe powder shown as vertical lines; (b) A plot showing the Variation of the cell parameters with the nominal atomic composition of $Pb_mSb_{2n}Te_{m+3n}$ nanocrystals following the Vegard's law, c) the EDS spectrum of Sample 1.

Fig. 4 (a-c) SEM images in different magnifications; (d) Diagrammatic sketch of Sample 1; (e) TEM and HRTEM images of Sample 1.

Fig. 5 X-ray photoelectron spectroscopy (XPS) spectra for the Sample 1 and Sample 3: (a) Survey of the two samples; (b) High-resolution XPS peaks of Pb (4f), (e) Sb (3d) and (f) Te (3d) regions; (c-d) Reference binding energies for PbTe and PbO are indicated at bottom.

Fig. 6 SEM images of samples synthesized under different temperature: (a-b) 120℃; (c) 140℃; (d) 200℃.

Fig. 7 SEM images of samples synthesized with different KOH amount (a-b) 0g (0mmol) , (c) 0.1g (1.79mmol) , (d) 1.5g (26.79mmol).

Fig. 8 SEM images of as-prepared samples synthesized in different amount of metal source: Sb source with (a-d) 0g; 1.0g; 1.5g; 2.0g; Pb source with (e, g, h) 0g; 1.0g; 1.5g; XRD pattern of as-prepared samples without Pb source.

Fig. 9 (a) Schematic illustration of the proposed growth mechanisms of the $Pb_{12..44}SbTe_{13.94}$ nanorods for hypothesis 1 (along black arrows with question marks) and hypothesis 2 (along red arrows); (b) the angles and relative position between Te-Te and the growth directions change during topological transformation from Te hexagonal phase to PbTe *fcc* phase.

Fig. 10 SEM images of samples obtained by solvothermal treatment after introducing Pb source and Sb source for different time intervals: (a) 0h, (c) 2h, (d) 4h, (d) 5.5h, (e) 8h, (h) 72h; (b) XRD pattern of Te nanorods synthesized at 0h; (f) Average length of Sample 1 nanorods decreased as compared to

that of Te nanorods.

Fig. 11 The tendency of Sample 1 crystals' morphologies from 1D nanorod/tube to 3D nanocubes as increasing the amount of KOH, time, temperature, respectively.

Fig. 12 Plot of $(\alpha hv)^2$ versus hv for determination of the band gap of Sample 1, Sample 2 and Sample 3 and the insets are correspond SEM images.

Figures

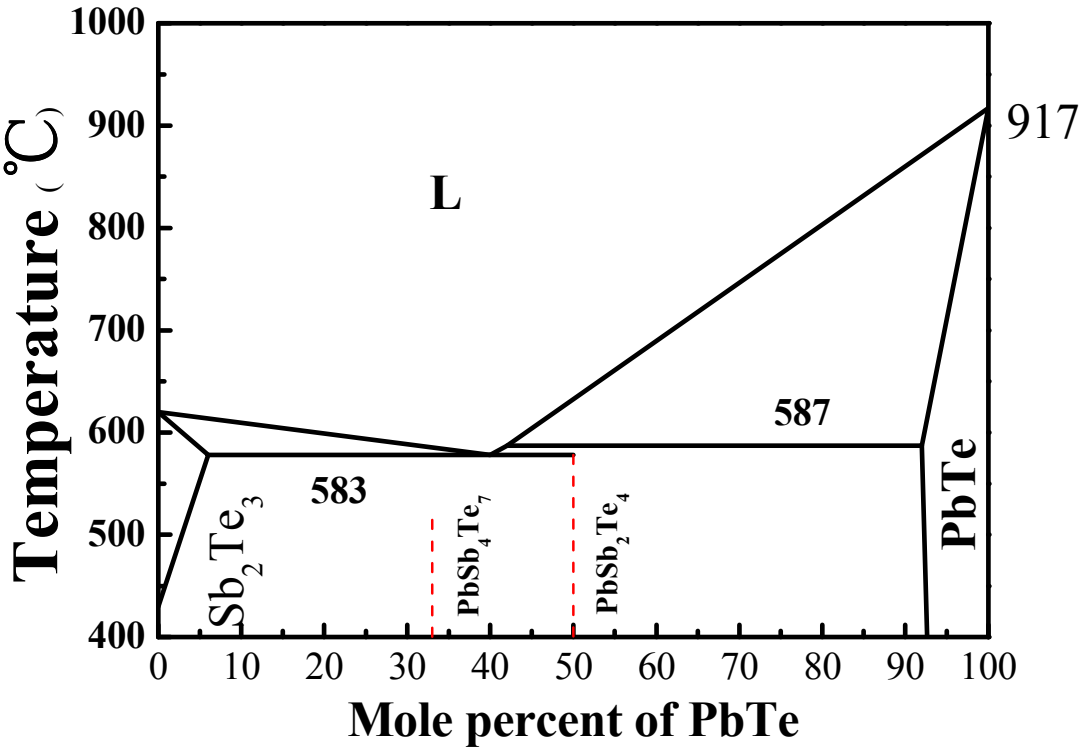

Fig. 1

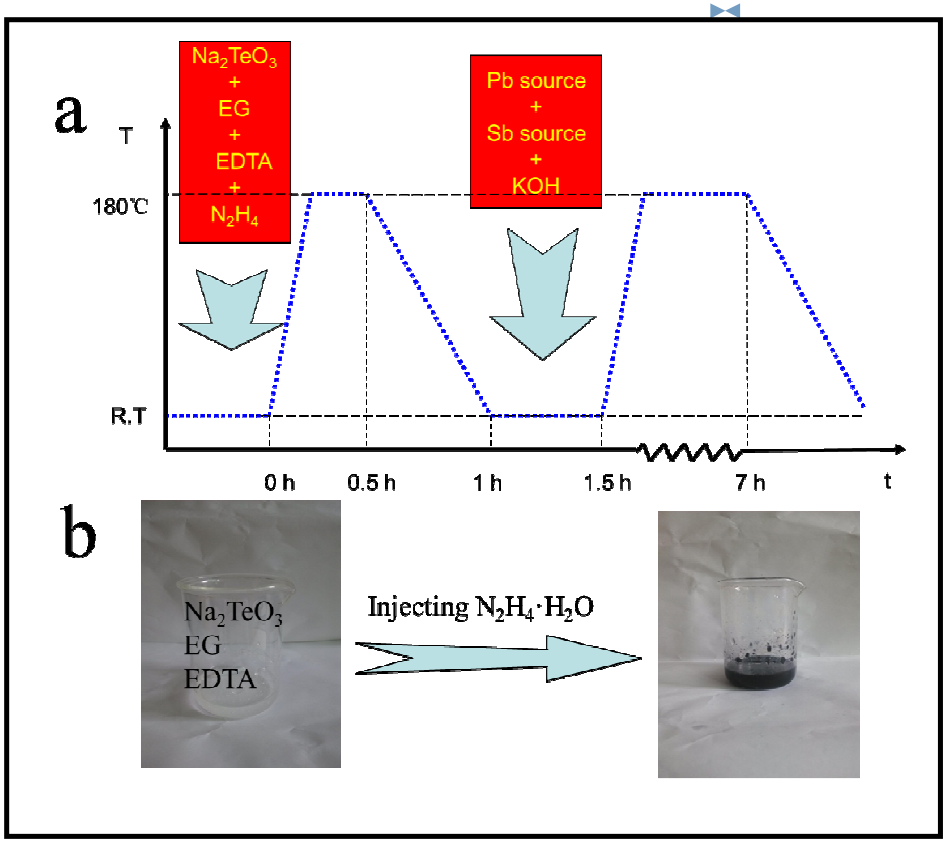

Fig. 2

Sample	Pb(at%)	Sb(at%)	Te(at%)	Composition	Lattice Parameter	Mole Sb/ Total Mole Sb+Pb
Sample 1	45.44	3.65	50.91	$Pb_{12..44}SbTe_{13.94}$	6.46142	0.074
Sample 2	41.19	7.05	51.76	$Pb_{5.84}SbTe_{7.34}$	6.45869	0.146
Sample 3	35.01	11.99	53.00	$Pb_{2.91}SbTe_{4.41}$	6.45558	0.256

Table. 1

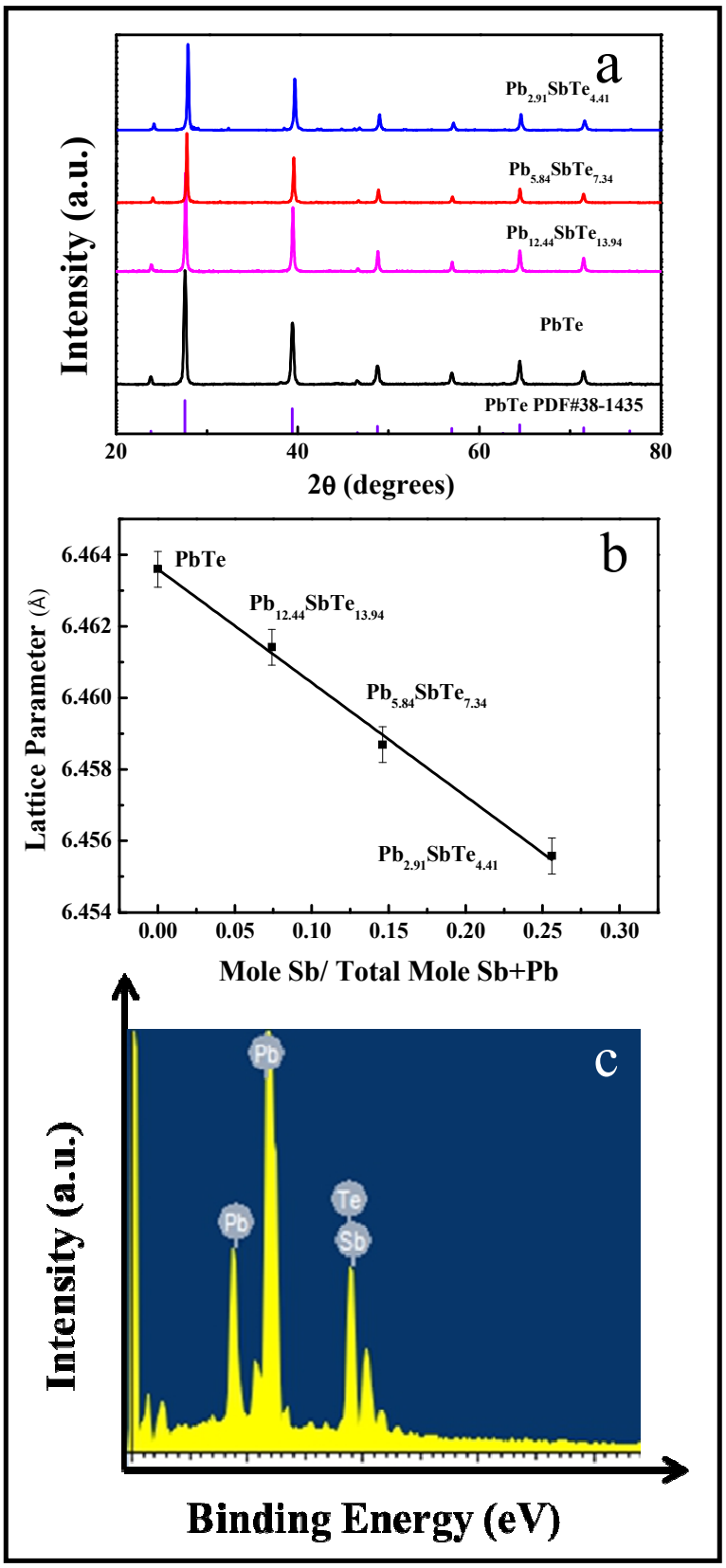

Fig. 3

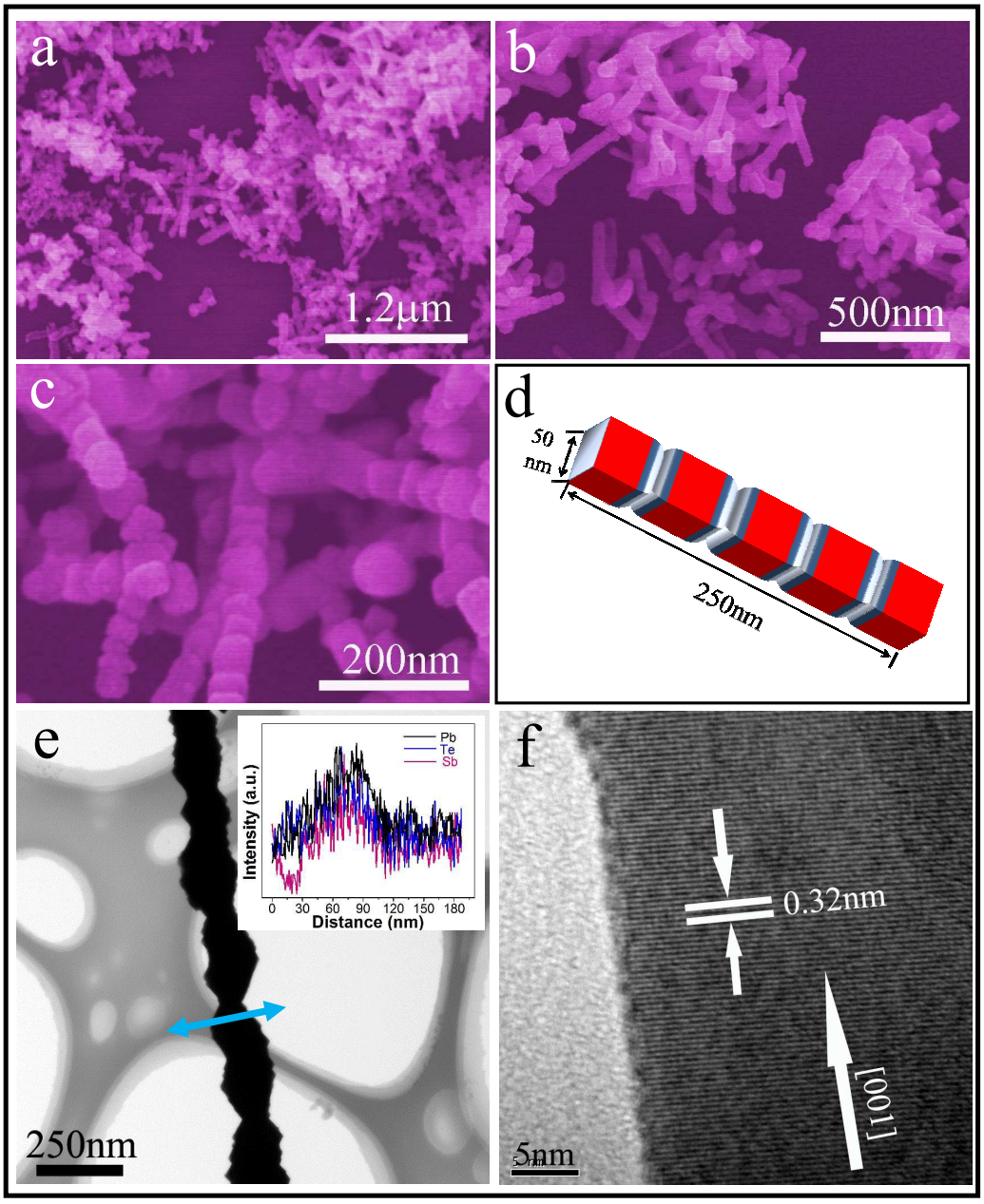

Fig. 4

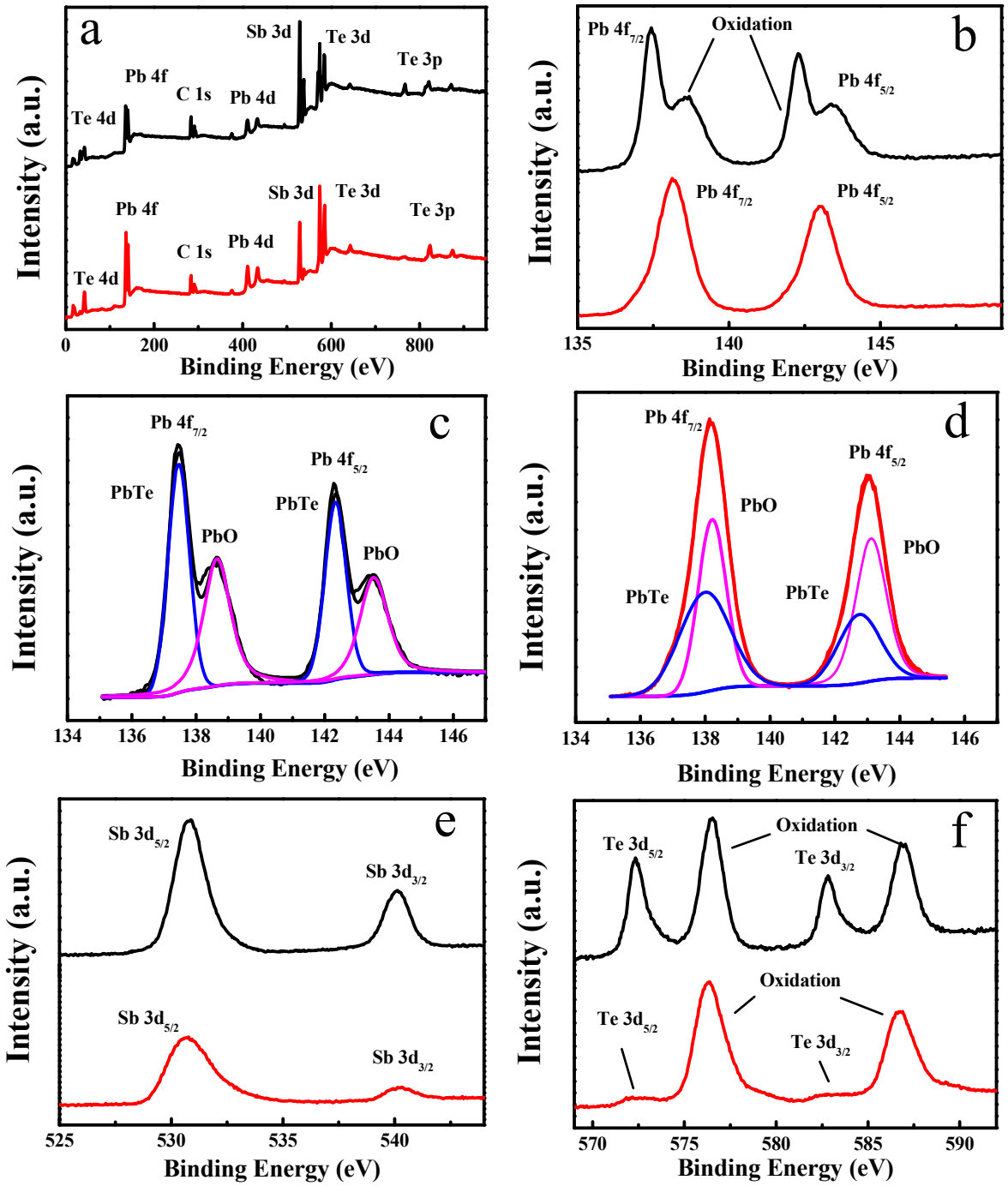

Fig. 5

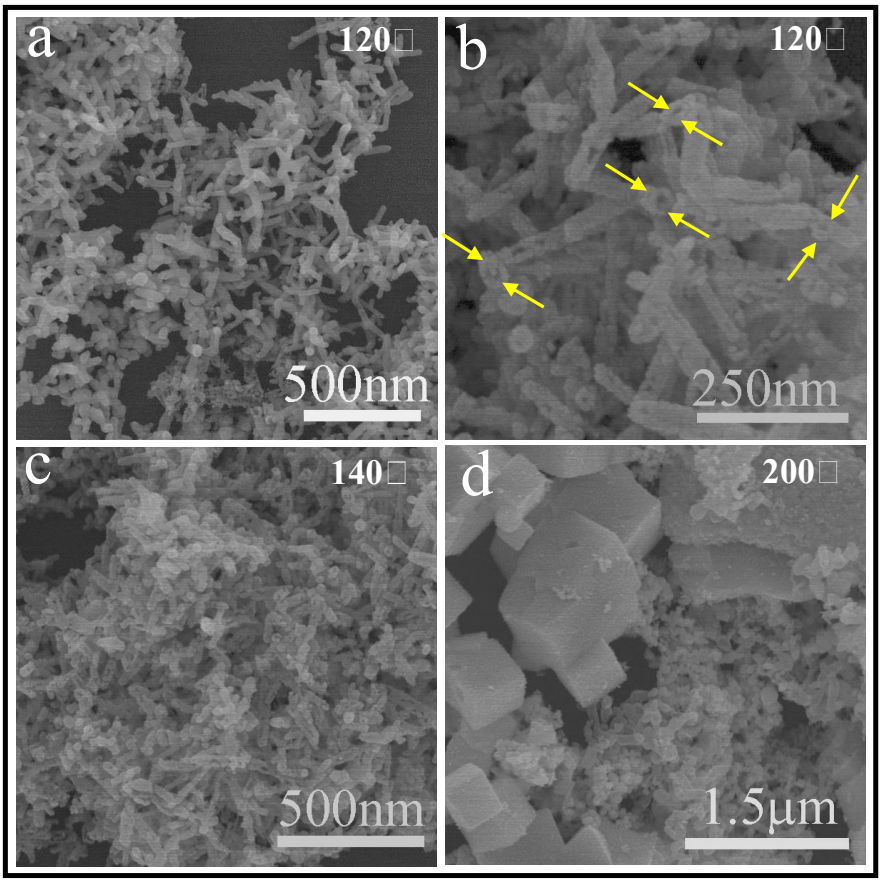

Fig. 6

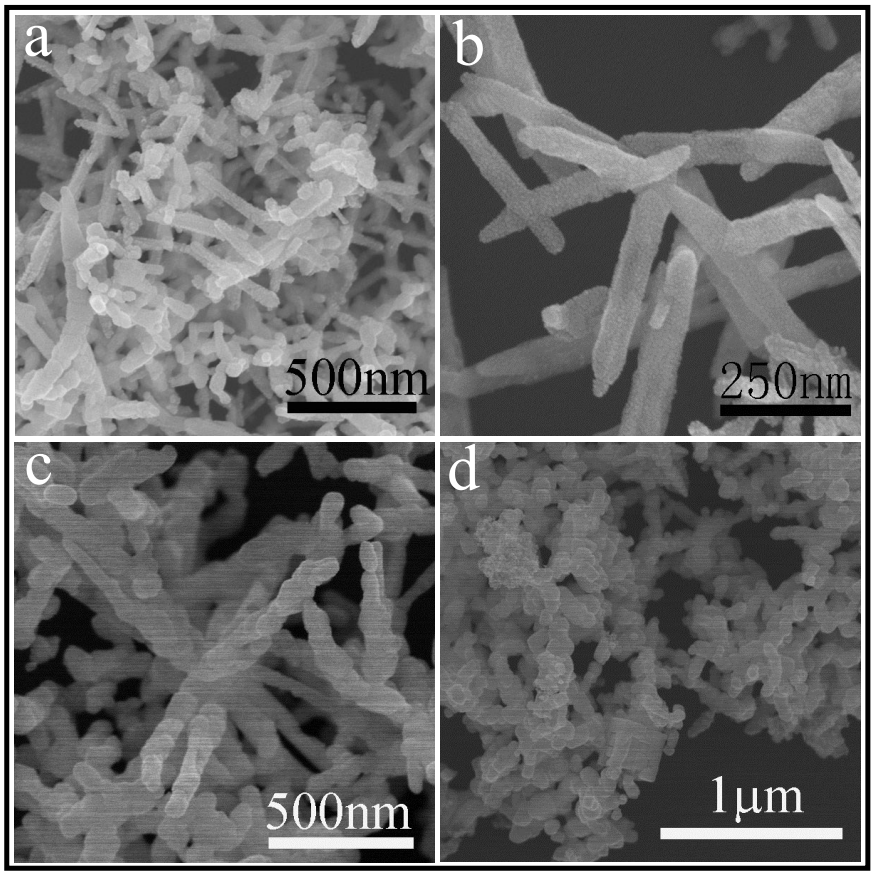

Fig. 7

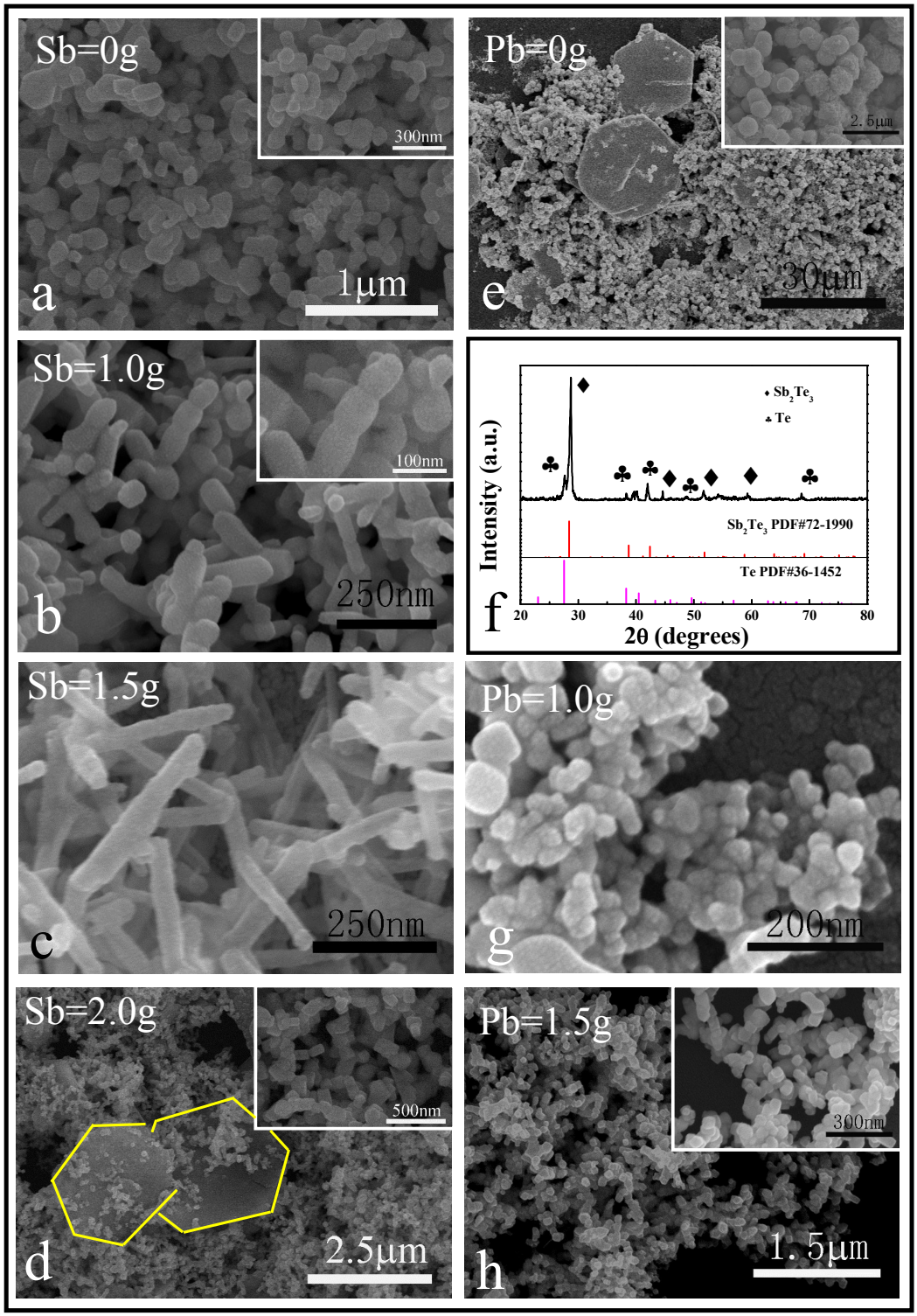

Fig. 8

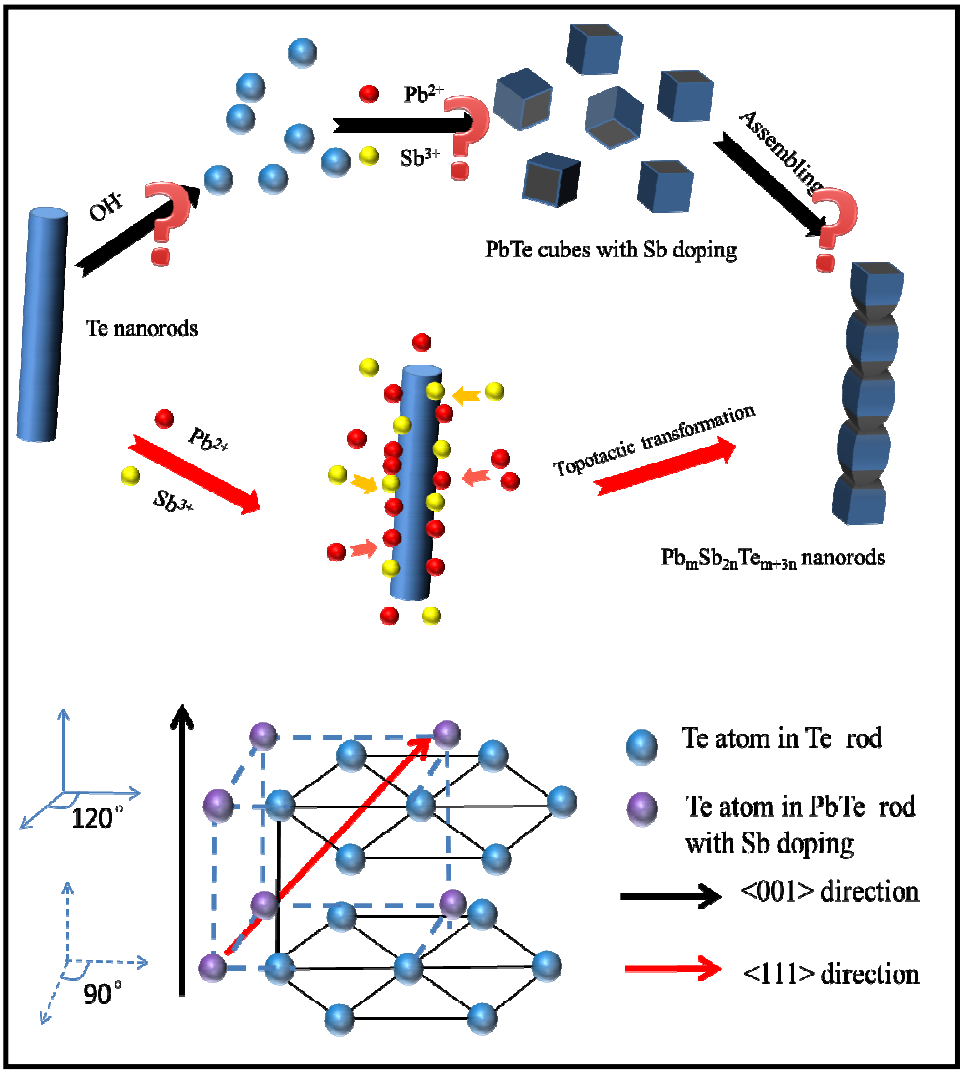

Fig. 9

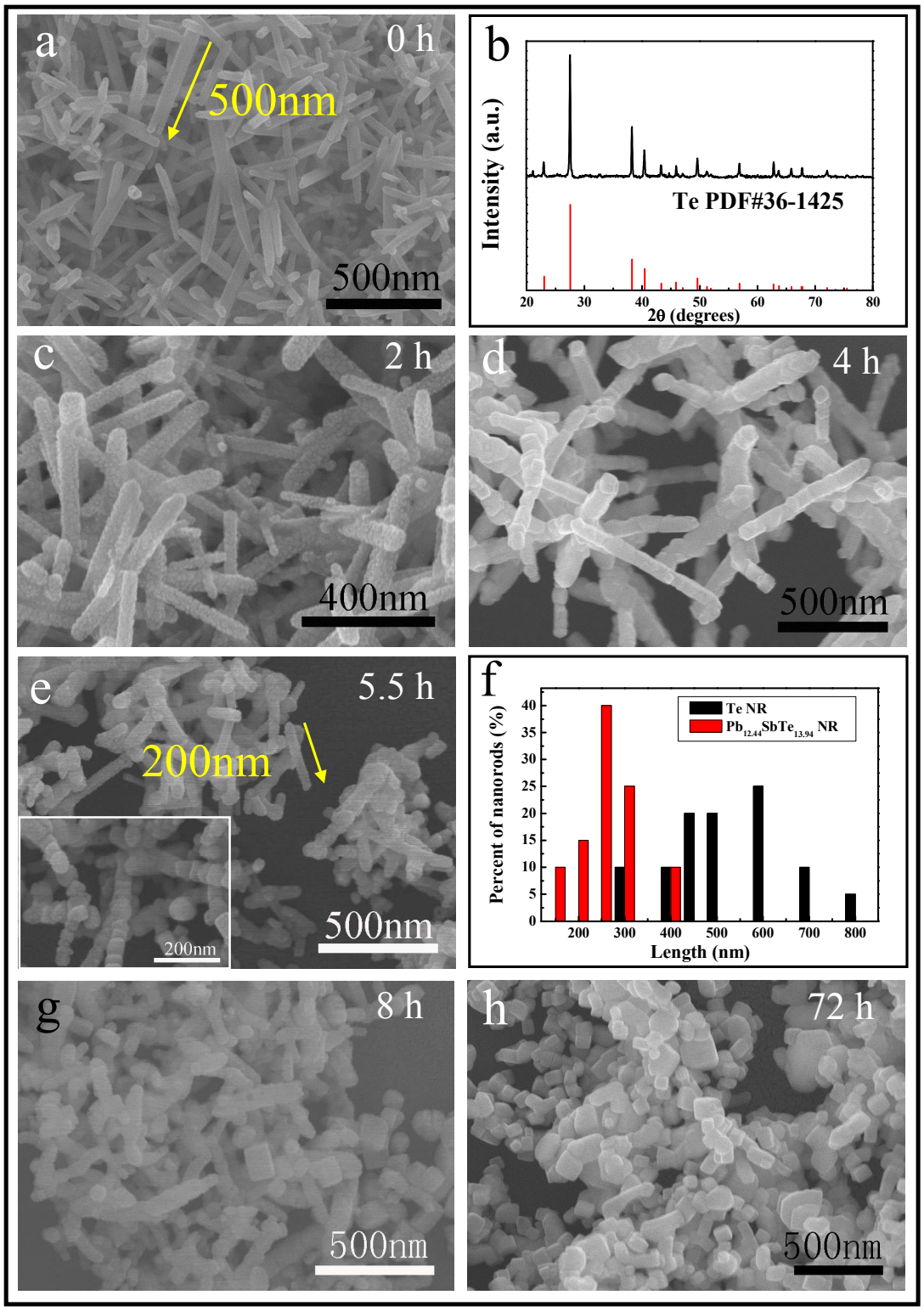

Fig. 10

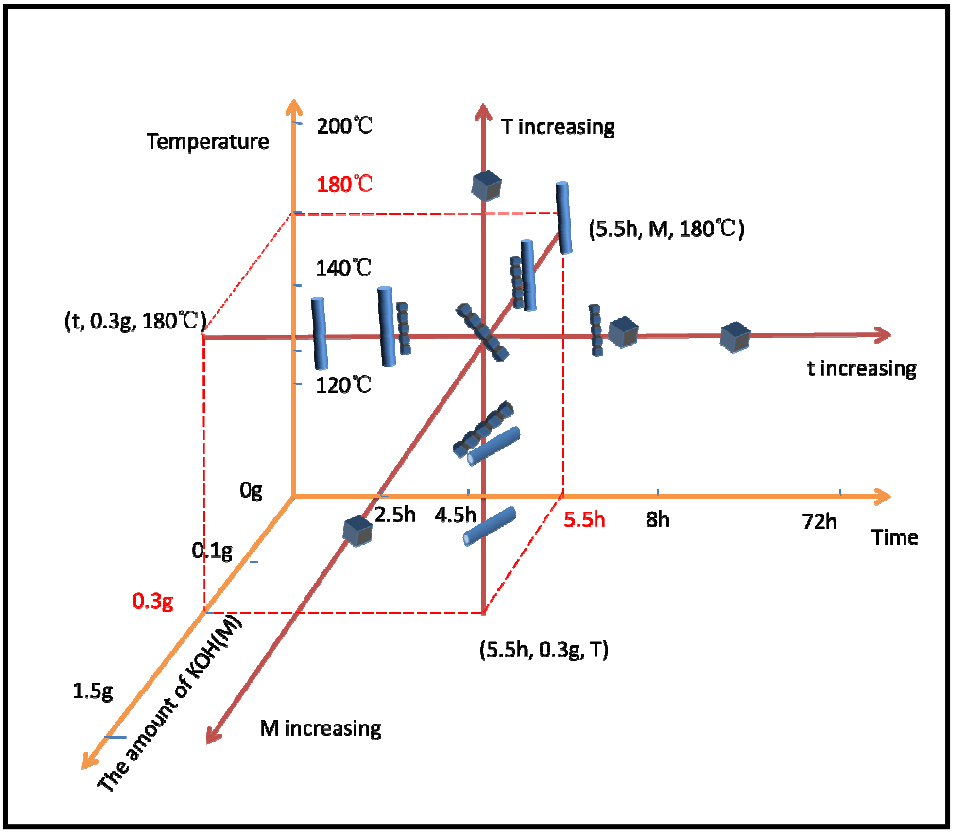

Fig. 11

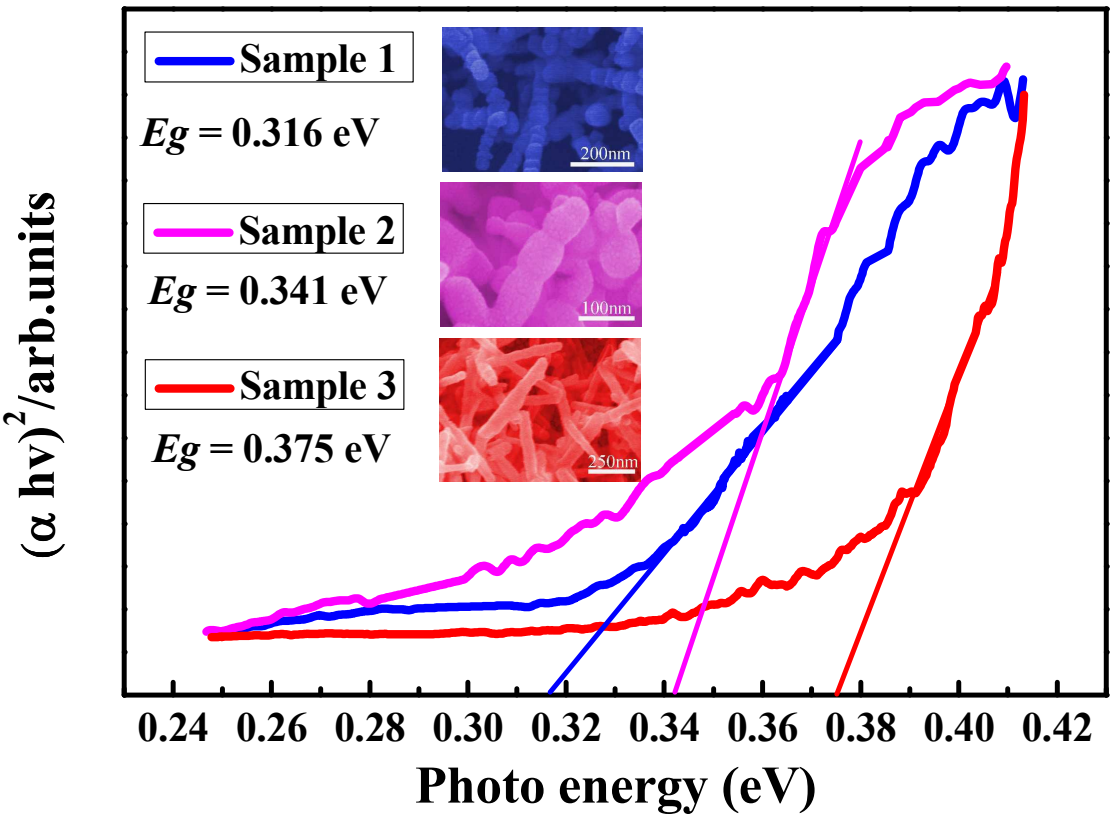

Fig. 12

Table of content

We have synthesized new phase $Pb_mSb_{2n}Te_{m+3n}$ nanorods using Te self-sacrifice template via Pb^{2+}/Sb^{3+} synergistic effect topotactic transformation. These samples show bigger band gap values than previously reported value for binary PbTe due to the strong quantum confinement effect.